

Article

An Insight to High Humidity-Caused Friction Modulation of Brake by Numerical Modeling of Dynamic Meniscus under Shearing

Liangbiao Chen ¹, Gang (Sheng) Chen ^{2,*} and Jen-Yuan (James) Chang ³

¹ Department of Mechanical Engineering, Lamar University, Beaumont, TX 77710, USA; E-Mail: liangbiao.chen@lamar.edu

² College of IT & Engineering, Marshall University, Huntington, WV 25755, USA

³ Department of Power Mechanical Engineer, National Tsing Hua University, Hsinchu 30013, Taiwan; E-Mail: jychang@pme.nthu.edu.tw

* Author to whom correspondence should be addressed; E-Mail: chenga@marshall.edu; Tel.: +1-304-634-3204.

Academic Editor: Jeffrey L. Streator

Received: 17 October 2014 / Accepted: 29 April 2015 / Published: 19 May 2015

Abstract: To obtain an insight to high humidity-caused friction modulation in brake pad-rotor interface, the adhesion phenomenon due to a liquid bridge is simulated using an advanced particle method by varying the shearing speed of the interface. The method, called generalized interpolation material point for fluid-solid interactions (GIMP-FSI), was recently developed from the material point method (MPM) for fluid-solid interactions at small scales where surface tension dominates, thus suitable for studying the partially wet brake friction due to high humidity at a scale of 10 μm . Dynamic capillary effects due to surface tension and contact angles are simulated. Adhesion forces calculated by GIMP-FSI are consistent with those from the existing approximate meniscus models. Moreover, the numerical results show that capillary effects induce modulations of adhesion as slip speed changes. In particular, the adhesion modulation could be above 30% at low speed. This finding provides insights into how the high humidity-caused friction could cause modulations of brake, which are unable to be achieved by conventional models. Therefore, the numerical analysis helps to elucidate the complex friction mechanisms associated with brakes that are exposed to high humidity environments.

Keywords: meniscus; adhesion; capillary; brake friction; MPM; fluid-solid interactions

1. Introduction

In the automotive brake industry, friction-induced noise and vibrations have been a critical cost factor because of customer dissatisfaction. Even though several decades of efforts have been made, friction-induced noise and vibrations still remain surprisingly unpredictable and poorly understood [1–3]. The extremely costly trial-and-error troubleshooting process has been applied for brake noise and vibration problems, despite that the numerical modeling and experiments were widely conducted. There are many unique dynamic phenomena and underlying mechanisms associated with friction-induced noise and vibrations. In a general sense, friction-induced noise and vibrations have time-varying, nonlinear stochastic features.

When a brake is soaked in high humidity environments, groan noise might occur, which is related to stick-slip due to the difference between static and dynamic frictions. For example, it is well known that many brakes can develop a noise problem called “morning sickness” during start-up running after parking overnight in fall or winter months when humidity could rise overnight and reach a high level of 90% in the cold morning. This kind of noise sustains for a short period only and will die away after the system warms up or dries up. It has been also reported that there exists high friction modulation associated with adsorbed water films, and the high humidity-caused coefficient of friction (cof) could be 50% higher than dry cof [4–10]. The effect of water vapor or moisture influence on cof has been observed by examining the humidity effect. As humidity increases, the cof may have larger variation during the initial sliding process which is attributed to surface tension. When mediated water film is not sufficient to fill the gap between the brake pad and rotor in a contact, the water film can fractionate into disjointed liquid bridges. In this situation, surface tension of the water at the menisci may strongly influence the contact force and accordingly friction between surfaces. Although many research works are dedicated to water-mediated friction, most existing research relied on conventional formulation of meniscus with certain modifications [11–15]. However, there has been lack of study on dynamic meniscus using comprehensive physics modeling. The classical theories of lubrication do not explain the dynamic adhesion force and the modulations as well as the associated friction variation generated in water bridges.

Conventional automotive brake friction materials are composites bonded with a phenolic resin reinforced with metallic or non-metallic fibers. Current automotive braking systems widely use two different kinds of brake lining materials: semi-metallic and non-asbestos organic (NAO). The surface of the brake pad has distributions of small pores which can retain moisture at ambient conditions. High friction due to high humidity could be developed due to capillary adhesive force for the interface with relatively smooth surface when water meniscus are substantially established. Table 1 shows typically measured parameters of a brake pad-disk interface which exhibited high friction induced noise problem under high humidity condition. It is noted that in most industry testing, the cof under high humidity environment is measured as an average value, as shown in Table 1.

It is noted that when temperature drops to zero, the dynamic viscosity of the water will be doubled [16]. When the water gets contaminated, the interface liquid viscosity could be up to 5–10 times

of the viscosity of distilled water. Moreover, when other liquids such as automobile engine oil or gear oil are mediated, the interface liquid viscosity could be up to 20 times of the viscosity of distilled water [17].

Table 1. Parameters of a brake pad-disk interface.

Parameter	Symbol	Value
Applied pressure on brake pad	p	2 MPa
Width of brake pad	B	50 mm
Length of brake pad	L	80 mm
Water-pad contact angle	θ	60°
Density of asperity peaks	N	$2.5 \times 10^{10} \text{ m}^{-2}$
Radius of asperity peaks	β	10 μm
RMS of brake pad roughness	σ_r	0.2 μm
Young's modulus of brake pad	E	150 GPa
Surface tension of water at 0–20 °C	γ	0.0728 N/m
Dynamic viscosity of distilled water at 20 °C	μ	$1.0 \times 10^{-3} \text{ Pa}\cdot\text{s}$
Dynamic viscosity of distilled water at 0 °C	μ	$1.8 \times 10^{-3} \text{ Pa}\cdot\text{s}$
Dynamic viscosity of contaminated water at 20 °C	μ	$\sim 1.0 \times 10^{-2} \text{ Pa}\cdot\text{s}$
Dry cof	η_d	0.30
High humidity-soaked cof	η_w	0.37

In this paper, we try to obtain a detailed understanding of the single meniscus effects during shearing by applying an advanced numerical approach developed for fluid-solid interactions with surface tension [18–21]. First, the formulations of the numerical method are introduced, emphasizing the surface tension model and contact angle treatment. Numerical analysis then is conducted to model the shearing of a micro-scaled water bridge. Numerical results of meniscus shapes and adhesion forces are presented. Discussions and conclusions are given at the end of the paper.

2. Advanced Material Point Method

Because of the complexity of the topology of fluid interface and the contact conditions between fluids and solids, analytical analysis becomes extremely difficult on solving fluid-solid interface problems involving surface tension. The high performance, recently emerging numerical approaches offer new opportunities to solve these problems accurately. Currently, there are limited numerical packages that are capable of tackling fluid-solid interface problems with surface tension. Most popular approaches do not incorporate surface tension when they are applied to fluid-solid interface problems. In this paper, an advanced particle method, called generalized interpolation material point for fluid-solid interaction (GIMP-FSI) [19,21], is used to simulate the friction behaviors of brake pad-rotor interface with a water meniscus. GIMP-FSI was built on the material point method (MPM) [22] and the generalized interpolation material point (GIMP) [23]. The method is devised to solve fluid-solid interactions with surface tension.

2.1. General Governing Equations

According to conservation of mass and momentum, the governing equations solved in the material point method are:

$$\frac{d\rho}{dt} + \rho \nabla \cdot \mathbf{v} = 0 \tag{1}$$

and

$$\rho \mathbf{a} = \nabla \cdot \boldsymbol{\sigma} + \rho \mathbf{b} \tag{2}$$

where ρ is the density, \mathbf{v} is the velocity, $\boldsymbol{\sigma}$ is the stress tensor, \mathbf{a} is the acceleration, \mathbf{b} is the specific body force. Note that both equations are valid for both fluid and solid materials in MPM, a key difference from the meshed-based solvers for FSI problems.

In MPM or GIMP-FSI, particles are used to store the material properties such as mass, stress, and velocity. For solving Equations (1) and (2), a background mesh is also used in GIMP-FSI as a scratch pad, a key difference from other particle methods such as SPH. The scratch is usually a regular Cartesian grid for computational convenience. A weak form of Equation (2) can be derived on each grid node i :

$$m_i \mathbf{a}_i = \mathbf{f}_i^{ext} - \mathbf{f}_i^{int} + \mathbf{f}_i^{sur} \tag{3}$$

in which m_i denotes the grid mass; \mathbf{a}_i the grid acceleration; \mathbf{f}_i^{ext} represents the grid external force, \mathbf{f}_i^{int} is the grid internal force, and \mathbf{f}_i^{sur} is the surface tension forces that are required for solving FSI problems at small scales.

In advanced MPM, all the state variables are stored in particles. Therefore, to solve Equation (3), an interpolation step is required to calculate the grid variables from particles:

$$m_i = \sum_p S_{ip}(\mathbf{x}_p) M_p \tag{4}$$

$$\mathbf{f}_i^{int} = M_p \sum_p \mathbf{G}_{ip}(\mathbf{x}_p) \cdot \boldsymbol{\sigma}_p^{sp} \tag{5}$$

$$\mathbf{f}_i^{ext} = \sum_p S_{ip}(\mathbf{x}_p) \mathbf{b}_p + \sum_p S_{ip}(\mathbf{x}_p) \boldsymbol{\tau}_p \tag{6}$$

in which S_{ip} is the interpolation function evaluated at particle position \mathbf{x}_p , \sum_p denotes summation over particles, $\mathbf{G}_i = \nabla S_{ip}$ is the gradient of the interpolation function, m_p is the particle mass, $\boldsymbol{\sigma}_p^{sp}$ is the specific stress tensor, \mathbf{b}_p is particle body force, and $\boldsymbol{\tau}_p$ is particle traction. Grid accelerations calculated from Equation (3) will then be interpolated back to particles to complete one computational cycle in the material point method [22,23].

2.2. Surface Tension and Contact Angle

Surface tension and contact angle effects can dominate fluid-solid interactions at small scales. In this situation, the surface tension term in Equation (3) cannot be neglected. According to [18], surface tension forces for fluid materials (with a superscript of f) can be calculated as:

$$\mathbf{f}_i^{sur,f} = V_c \frac{\sigma \kappa}{[m]} \frac{m_i^f}{\langle m \rangle} (\nabla m_i^f) \tag{7}$$

in which V_c is cell volume, σ is surface tension coefficient, $[m]$ is density difference at the fluid interface, $\langle m \rangle$ is average density of the fluid interface, and κ is the curvature.

To correctly evaluate the responses of solid materials, a surface tension force $\mathbf{f}_i^{sur,s}$ must be added on the triple point of the solid-fluid surface [19,21], as:

$$\mathbf{f}_i^{sur,s} = (\sigma l_c) \mathbf{t}^f \tag{8}$$

in which l_c is the wetting length and the \mathbf{t}^f is the interface tangents.

The contact angle is an important wetting parameter which assesses the intensity of the phase contact between liquid and solid substances. To obtain contact angles between fluids and solids, a static contact angle θ_{eq} is used to recalculate the fluid normal near the contact line, as:

$$\mathbf{n}_{eq} = \mathbf{n}^s \cos \theta_{eq} + \mathbf{t}^s \sin \theta_{eq} \tag{9}$$

in which \mathbf{n}^s and \mathbf{t}^s is the solid normal and solid tangent, respectively. Modifications to fluid normal create a driven force to fluid so that a correct contact angle can be achieved [18–21].

3. Numerical Analysis of the Shearing of a Micro-Scaled Water Bridge

3.1. Problem Description

This study focuses on water meniscus effects without consideration of solid contact and chemical and other physical changes of the interface. Under the shearing operation of a slightly wet interface with meniscus, the pad and rotor may form numerous water bridged contact, in which surface tension results in a pressure difference across a meniscus surface referred to as capillary pressure or Laplace pressure. The adhesion developed due to capillary effect could be significant. If the adhesion value is close to the order of the magnitude of normal operation load, it could have substantial effect on the friction on the brake.

As shown in Figure 1, a 2D water droplet is placed between pad and rotor with a gap of 10 μm so that a water thin film is formed at static state. The initial width of water droplet is 30 μm . The top rotor is allowed to move with a speed from 0 to 5 m/s, while the bottom pad is fixed in both directions. For the case with surface tension, a meniscus will be evolved with a surface tension coefficient of 0.072 N/m and a contact angle of 60°. The effects of the surface tension will be evaluated by comparing with the case without surface tension, as shown in Figure 1b.

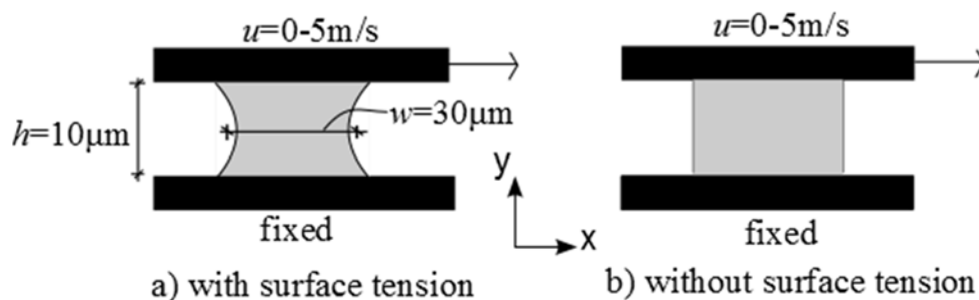


Figure 1. Geometry and boundary conditions for simulating a thin water film between pad and rotor.

3.2. Constitutive Models and Numerical Setup

To simulate thin film problem Figure 1, the following constitutive law is used for water:

$$\boldsymbol{\sigma} = -p\mathbf{I} + 2\mu\mathbf{d}' \quad (10)$$

in which μ is the dynamic viscosity, \mathbf{d}' is the rate of deformation tensor, and p is the hydrostatic pressure determined by an equation of state [22–25]:

$$p = K \left[\left(\frac{\rho}{\rho_0} \right)^\gamma - 1 \right] \quad (11)$$

in which K is the bulk modulus, γ is a material constant, ρ is the density and ρ_0 is the initial density. In this study, we used $\mu = 1.0 \times 10^{-2}$ Pa·s, $K = 2.2 \times 10^9$ Pa, and $\rho_0 = 1000$ kg/m³, which are based industrial practice. The constitutive law for solid is based on the compressible Neo-Hookean hyperplastic model [26], as:

$$\boldsymbol{\sigma} = -KJ(J-1)\mathbf{I} + GJ^{-2/3}\text{dev}(\mathbf{b}) \quad (12)$$

in which J is the determinant of the deformation tensor \mathbf{F} , K the bulk modulus, G is the shear modulus, $\mathbf{b} = \mathbf{F}\mathbf{F}^T$ is the left Cauchy stress tensor, and “dev” means deviatoric stress. For the solid material, we adopted $K = 8.9 \times 10^9$ Pa and $G = 3.852 \times 10^9$ Pa.

Figure 2 shows the initial configuration of the problem in GIMP-FSI. A 50×20 mesh is used for a 50×20 μm domain, with a period boundary condition applied at both end of x direction. A total of 1200 fluid particles and 2000 solid particles are used to simulate the water thin film and the belts, respectively. The same numerical setup will be used for the case with surface tension and contact angle effect, as well as the case without considering surface tension and the contact angle.

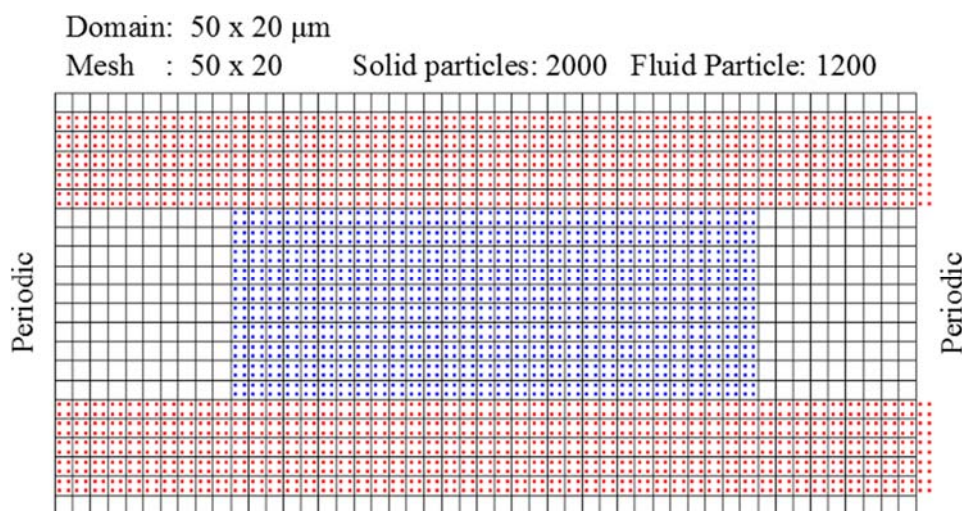


Figure 2. Numerical Setup in GIMP-FSI.

The simulation is conducted by implementing GIMP-FSI in Uintah framework which has been benchmarked [19–23,27]. The boundary condition is applied to the upper pad so that it accelerates from 0 m/s to 5 m/s in 4×10^{-3} milliseconds. The size of time step is an order of 1×10^{-10} , which is changed

automatically by the program based on Courant-Friedrichs-Lewy conditions. A total of 12 CPUs were used to obtain computational results within 4 hours.

3.3. Numerical Results

Figure 3 shows numerical results from GIMP-FSI for the problem described in Section 3.1. Two different cases were simulated. For the case without surface tension and contact angle effects (the left column of Figure 3), the water thin film starts as a rectangular shape (at $t = 0$) and gradually deforms due to the moving of the top rotor. However, when surface tension and contact angle are considered, the thin film is first allowed to form a meniscus (at $t = 0$ for the right column of Figure 3) with a static contact angle between the water film and two solid materials. When the top rotor starts moving, the meniscus will change accordingly, as shown in the right column of Figure 3.

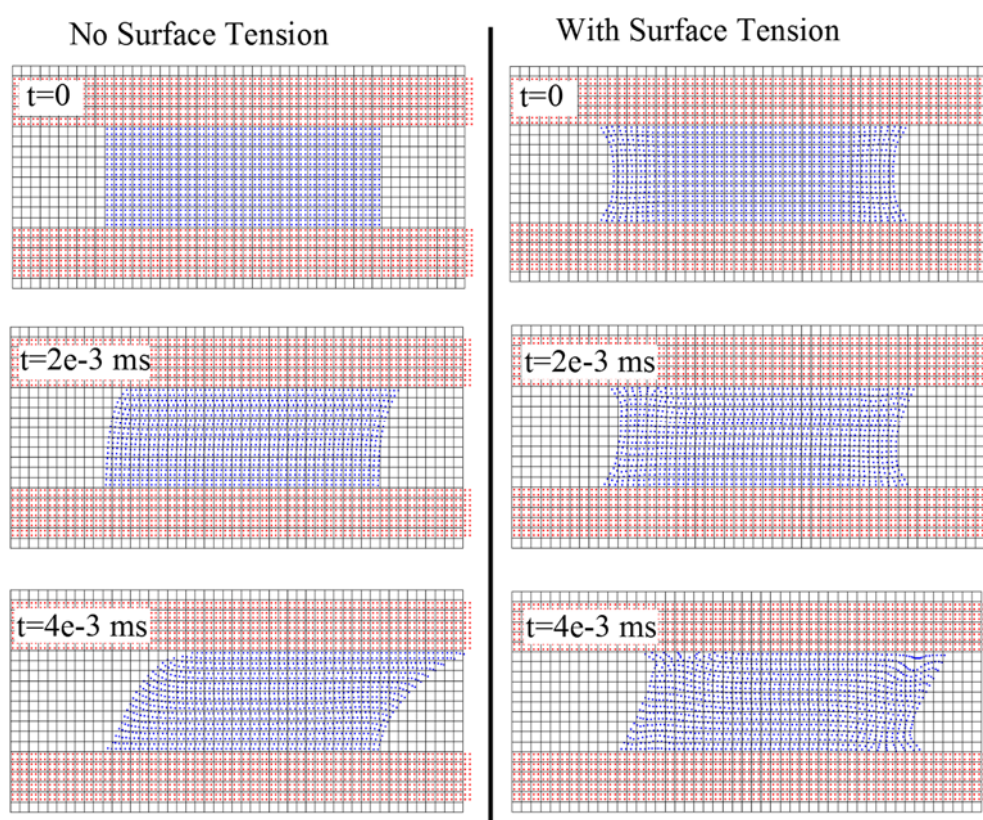


Figure 3. Results from GIMP-FSI for dynamic meniscus (with and without surface tension).

Figure 4 shows the dynamic adhesion force between rotor and pad against slip speeds. The adhesion forces, normal reaction forces in the y direction, are recorded during the pad slips (at every time step). It can be seen that the magnitude of the adhesion forces increase as the slip speed/time goes up for both cases (without surface tension and that with surface tension). However, the surface tension generates greater adhesion forces compared to the case without surface tension, which might exert more friction if the top rotor directly contacts the bottom pad. In addition, the presence of surface tension and contact angle effect causes strong modulation in the adhesion forces. The adhesion modulation is above 30% at low speed, and gradually decreases till the speed reaches 2 m/s. Since the meniscus begins to deform after the speed reaches 2 m/s, the contact angle is not static anymore, thus causing greater modulation

in adhesion forces. This finding is generally consistent with the existing observations of high humidity-caused brake friction modulations, which, however, are unable to be explained by conventional models. Note that the simulation becomes unstable when liquid bridge breaks up around 4×10^{-3} milliseconds (corresponding slip velocity is 5 m/s). Therefore, adhesion forces after 4×10^{-3} are less reliable and are not presented here. Future work will be conducted to enable GIMP-FSI for analyzing adhesion forces after liquid bridge breaks up.

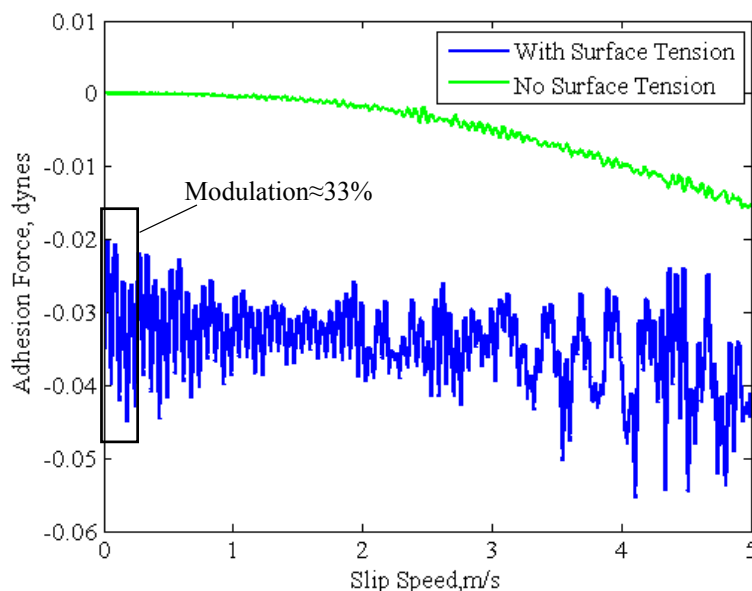


Figure 4. Adhesion (normal) forces vs. slip speed.

4. Discussions and Conclusions

A water bridge between two solids was simulated by the material point method to obtain a detailed analysis of the characteristics of adhesion developed in a water bridge, so as to obtain insight for friction characteristics of a brake interface exposed to huge humidity environments. With the GIMP-FSI method, adhesion forces are calculated by considering both surface tension and contact angle effects. The simulation was performed with varied shearing speeds. The results show that the adhesion forces caused by surface tension are much higher than the case without surface tension. This leads to a change in the normal force between interface and eventually affects the friction behavior. Moreover, the adhesion force by considering surface tension exhibits a modulation with respect to slide speed change, which could be above 30% at low slip speed. Accordingly, this could result in the increase and modulation of friction forces, as the contact force is changed by adhesion.

For the static case, the obtained results are consistent with that obtained from conventional meniscus model. For the sliding case, the obtained results are not only consistent with that obtained from existing dynamic meniscus models, but also offer a quantitative result of the modulation of adhesion, which directly validates the modulation of friction in high humidity environment reported by the brake system community. This result helps the understanding of the characteristics of the modulation of friction with water bridge. Therefore, the proposed approach can be further extended to be used for friction analysis of interface in high humidity environment.

Even though we focus on modeling a single meniscus in a micro level in this study, we can extend the approach to the cases with multiple-contact of pad-rotor contact without or with asperities. The developed meniscus/adhesion modeling can be integrated into the friction model to quantify the characteristics and variation of friction under high humidity conditions. In general, given the interplanar separation, the mean peak radius of asperity, the thickness of the water film, the surface tension, the water contact angle between water and surface, and the total number of summits, the macro-meniscus force can be solved. The proposed approach helps to interpret the complex phenomena of friction in high humidity environment encountered in an automotive brake system.

Acknowledgments

The authors acknowledge Xian Zheng in Futon Motor Company and Li Lee in Akebono Company for their guidance and support in this study.

Conflict of Interest

The authors declare no conflict of interest.

References

1. Chen (Sheng), G. *Vehicle Noise, Vibrations and Sound Quality*; SAE International Publishing: Warrendale, PA, USA, 2012.
2. Chen, F.; Tan, C.A.; Qualia, R.L. *Break Squeal: Mechanism, Analysis, Evaluation and Reduction/Prevention*; SAE International Publisher: Warrendale, PA, USA, 2006.
3. Eriksson, M.; Bergman, F.; Jacobson, S. On the nature of tribological contact in automotive brakes. *Wear* **2002**, *252*, 26–36.
4. Kobayashi, M.; Odani, N. Study on Stabilization Friction Coefficient of Disk Brake Pads in Cold Condition. *SAE Tech. Paper* **1997**, doi:10.4271/973030.
5. Eriksson, M.; Lundqvist, A.; Jacobson, S. A study of the influence of humidity on the friction and squeal generation of automotive brake pads. *J. Automob. Eng.* **2001**, *215*, 329–342.
6. Lee, J.H.; Sheng, G.; Chang, J.Y. Micro-tribological interface model for friction-induced cold start-up running dynamics. *Microsyst. Technol.* **2012**, *18*, 1469–1479.
7. Brecht, J.; Schiffner, K. Influence of Friction Law on Brake Creep Groan. *SAE Tech. Papers* **2001**, doi:10.4271/2001-01-3138.
8. Lee, K.; Blau, P.J.; Truhan, J.J. Effects of moisture adsorption on laboratory wear measurements of brake friction materials. *Wear* **2007**, *262*, 925–930.
9. Bhushan, B. *Principles and Applications of Tribology*; John Wiley & Sons: Hoboken, NJ, USA, 1999.
10. Tian, X.; Bhushan, B. The Micro Meniscus Effect of Thin Liquid Film on the Static Friction of Rough Surface Contact. *J. Phys. D Appl. Phys.* **1996**, *29*, 163–178.
11. Zheng, J.; Streater, J.L. A micro-scale liquid bridge between two elastic spheres: Deformation and Stability. *Tribol. Lett.* **2003**, *15*, 453–464.

12. Xue, X.; Polycarpou, A.A. An improved meniscus surface model for contacting rough surfaces. *J. Colloid Interface Sci.* **2007**, *311*, 203–211.
13. Bhushan, B.; Kotwal, C.A. Kinetic meniscus model for prediction of rest stiction. *ASME Trans. Tribol.* **1998**, *120*, 42–50.
14. Liu, B.; Sheng, G.; Lim, S. Meniscus force modeling and study on the fluctuation of stiction/friction force in CSS test process. *IEEE Trans. Magn.* **1997**, *33*, 3121–3123.
15. Matsuoka, H.; Matsumoto, S.; Fukui, S. Dynamic meniscus models for MEMS elements. *Microsyst. Technol.* **2005**, *11*, 1132–1137.
16. Kestin, J.; Sokolov, M.; Wakeham, W. Viscosity of liquid water in the range $-8\text{ }^{\circ}\text{C}$ to $150\text{ }^{\circ}\text{C}$. *J. Phys. Chem. Ref. Data* **1978**, *7*, 941–946.
17. SAE Oil Standard. Available online: <http://topics.sae.org/fuels-energy-sources/standards/> (accessed on 2 April 2013).
18. Chen, L.; Lee, J.H.; Chen, C.-F. On the modeling of surface tension and its applications by the generalized interpolation material point method. *CMES Comput. Model. Eng. Sci.* **2012**, *86*, 199–223.
19. Chen, L. Using the Generalized Interpolation Material Point Method for Fluid-Solid Interactions Induced by Surface Tension. Ph.D. Dissertations, University of Alaska, Fairbanks, USA, December 2013.
20. Chen, L.; Lee, J.H.; Chen, C.-F. Using the Generalized Interpolation Material Point Method for Compressible Flows at Low Reynolds Numbers. *CMES Comput. Model. Eng. Sci.* **2014**, in press.
21. Chen, L.; Lee, J.H.; Chen, C.-F. Using the Generalized Interpolation Material Point Method for Fluid-Solid Interactions Induced by Surface Tension. *CMES Comput. Model. Eng. Sci.* **2013**, in press.
22. Sulsky, D.; Zhou, S.J.; Schreyer, H.L. Application of a particle-in-cell method to solid mechanics. *Comput. Phys. Commun.* **1995**, *87*, 236–252.
23. Bardenhagen, S.; Kober, E. The generalized interpolation material point method. *CMES Comput. Model. Eng. Sci.* **2004**, *5*, 477–495.
24. Morris, J.P.; Fox, P.J.; Zhu, Y. Modeling low Reynolds number incompressible flows using SPH. *J. Comput. Phys.* **1997**, *136*, 214–226.
25. Monaghan, J.J. Simulating free surface flow with SPH. *J. Comput. Phys.* **1994**, *110*, 399–402.
26. Simo, J.C.; Hughes, T.J.R. *Computational Inelasticity*; Springer-Verlag: New York, NY, USA, 1998.
27. Parker, S.; Guilkey, J.; Harman, T. A component-based parallel infrastructure for the simulation of fluid-structure interaction. *Eng. Comput.* **2006**, *22*, 277–292.